Highly controllable near-surface swimming of magnetic Janus nanorods: application to payload capture and manipulation

2011 J. Phys. D: Appl. Phys. 44 125001

(http://iopscience.iop.org/0022-3727/44/12/125001)

J. Phys. D: Appl. Phys. **44** (2011) 125001 (9pp) doi:10.1088/0022-3727/44/12/125001

Highly controllable near-surface swimming of magnetic Janus nanorods: application to payload capture and manipulation

Lamar O Mair[1], Benjamin Evans[2], Adam R Hall[3], Jerome Carpenter[1], Adam Shields[4], Kris Ford[5], Michael Millard[5] and Richard Superfine[4]

[1] Curriculum in Applied Sciences and Engineering, University of North Carolina at Chapel Hill, NC 27599, USA
[2] Department of Physics, Elon University, Elon, NC 27244, USA
[3] Joint School of Nanoscience and Nanoengineering, University of North Carolina at Greensboro, NC 27401, USA
[4] Department of Physics and Astronomy, University of North Carolina at Chapel Hill, NC 27599, USA
[5] Department of Biomedical Engineering, University of North Carolina at Chapel Hill, NC 27599, USA

E-mail: rsuper@physics.unc.edu

Received 3 December 2010, in final form 2 January 2011
Published 10 March 2011
Online at stacks.iop.org/JPhysD/44/125001

Abstract
Directed manipulation of nanomaterials has significant implications in the field of nanorobotics, nanobiotechnology, microfluidics and directed assembly. With the goal of highly controllable nanomaterial manipulation in mind, we present a technique for the near-surface manoeuvering of magnetic nanorod swimmers and its application to controlled micromanipulation. We fabricate magnetic Janus nanorods and show that the magnetic rotation of these nanorods near a floor results in predictable translational motion. The nanorod plane of rotation is nearly parallel to the floor, the angle between rod tilt and floor being expressed by θ, where $0^\circ < \theta < 20^\circ$. Orthogonal magnetic fields control in-plane motion arbitrarily. Our model for translation incorporates symmetry breaking through increased drag at the no-slip surface boundary. Using this method we demonstrate considerable rod steerability. Additionally, we approach, capture, and manipulate a polystyrene microbead as proof of principle. We attach Janus nanorods to the surfaces of cells and utilize these rods to manipulate individual cells, proving the ability to manoeuver payloads with a wide range of sizes.

S Online supplementary data available from stacks.iop.org/JPhysD/44/125001/mmedia

(Some figures in this article are in colour only in the electronic version)

1. Introduction

Producing micro- and nano-scale machines capable of directed locomotion and payload manipulation is a principal goal of nanotechnology [1–12]. Specifically, micro- and nano-scale motors and machines capable of directed locomotion and payload manipulation in a variety of low Reynolds number (low-Re) solutions hold potential for manipulating and assembling objects at the nano-scale by making use of hydrodynamic methods of self-propulsion [13–20]. Magnetically driven devices capable of being guided by externally applied magnetic fields [17, 21] are particularly useful, as these micro-objects can perform complex manoeuvers without carrying any onboard fuel [18, 20, 22]. Swimming in a low Reynolds number environment requires a mechanism which breaks the symmetry of the swimmer's motion [23, 24]. Many different types of swimmers have been proposed and demonstrated, such as three-bead swimmers [23, 25, 26], rotating helices [14, 17], linked-bead swimmers [21], flexible magnetic filaments [27, 28] and membranes [29].

Most recently, assemblies of micrometre-sized magnetic beads have been rotated near a wall in an end-over-end fashion; the hydrodynamic conditions of the sphere near the wall break the symmetry of the rotation and result in a net translation of the micro-object [16, 18, 22, 20]. Additionally, Zhang *et al* rotated solid Ni nanorods in a plane perpendicular to the floor surface and observed crawling motion [15]. Significantly, all crawling mechanisms demonstrated to date rotate the beads or rods in a plane oriented perpendicularly to the hydrodynamically relevant surface (floor). In this work we present a simple, efficient method for the fabrication and manipulation of nanorod swimmers which operate via rotation in a plane nearly parallel to the floor, sweeping out a large area in a nearly horizontal plane. This is the first demonstration of high-aspect-ratio hydrodynamic swimming for which the long axis of the nano-object lies nearly parallel to the floor.

We implement this method of translation using magnetic Janus nanorods. Janus nano- and micro-scale particles are unique in that they embody some form of surface anisotropy. The term (named after the god in Roman mythology who possessed two faces) was originally coined by Casagrande and Veyssie [30] and is typically used to describe particles having two sides which differ in some interfacial manner. Previous work has successfully used template-directed electrodeposition to create nanorods with a diverse array of compositions along their lengths [31–35]. Additionally, Qin *et al* developed a technique for modifying rods along the rod radius for single-molecule electrical measurements [36, 37], catalytically driven nanorotors [38, 39] and nanodisc barcodes [40]. In this study, we fabricate magnetic Janus nanorods through a two-step process of templated electrodeposition (Au nanorod growth) and post-growth thermal evaporation of magnetic layers (Ni or Ni–Pd). Although solid magnetic rods will exhibit similar crawling behaviour, these magnetic Janus rods enable the additional benefit of regio-specific chemical functionalization due to the possibility of having, on a single nanorod, two or more exposed metals for surface functionalization. We selectively functionalize exposed Au regions with dangling thiol bonds to approach, capture and manoeuver AuPd-coated 1 μm polystyrene (PS) spheres. Additionally, we incubate magnetic Janus rods with human bronchial epithelial cells (HBE-16) and successfully manipulate these cells via rotational manoeuvering using individual rods. This work represents the first demonstration of magnetically responsive Janus nanorods, implements these rods as near-surface nano-swimmers capable of payload capture and manipulation, and models the swimming action mechanism using resistive force theory.

2. Experimental section

2.1. Janus nanorod fabrication

Template-based techniques for fabricating nanorods and nanotubes have been described elsewhere [35, 41, 42]. Briefly, we form Au nanorods by electrodeposition into the pores of commercially available Whatman anodized aluminium oxide (AAO) templates with nominal pore diameters of 200 nm. Templates are prepared by thermal evaporation of a Ag working electrode (450 nm thickness) onto one side of the template. Following this, templates are placed in a custom-made electrodeposition cell and deposition is performed using a standard three-electrode setup (Pt auxiliary electrode, Ag/AgCl reference electrode, thermally evaporated Ag working electrode). For this work, Au nanorods are grown to a length of approximately 5.5 μm; however, the technique we present is amenable to a wide variety of rod dimensions and compositions. Following rod electrodeposition, the Ag working electrode is etched in HNO_3 and the rods are released from the template via AAO dissolution in 1M NaOH. Released nanorods are rinsed 5 times in ethanol via sonication and gentle centrifugation, then dispersed in ethanol at a concentration of approximately 2.5×10^7 rods ml^{-1} (based on calculations of template pore density and deposition surface area).

Janus layer formation is performed via the thermal evaporation process shown in figure 1(*a*). A Si substrate is prepared with a Cr adhesion layer and Au nanorods are deposited onto it. Thermal evaporation is then used to deposit a 50 nm Ni film and a 15 nm Pd film. The total thickness of these layers is limited to roughly half the nanorod diameter to avoid total encapsulation of the rods. In the current experiments, Ni–Pd layers are used due to the high susceptibility of thermally evaporated Ni layers and their resistance to oxidation and chemical dissolution. Bead capture experiments (discussed later) are performed using only Ni Janus layers. Significantly, this technique is amenable to engineering the deposited layers with respect to composition, thickness and sequence ordering. We found similar results, for example, with Ni–Cu layers. Finally, the substrate is sonicated for 10 s at 12 W in isopropanol (IPA), causing the partially coated (Janus) Au rods to be removed from the surface and dispersed in solution. Scanning electron microscopy of the substrate surface after a partial removal of Janus nanorods is shown in figure 1(*b*). Voids left in the Ni–Pd thin film indicate the positions of nanorods that have been removed into solution, each rod now possessing a partial magnetic coating.

2.2. Nanorod manipulation

In order to collect video data of Janus nanorod manipulation, we dilute $\sim 1 \times 10^7$ rods in 20 ml of 1 : 1 deionized water and isopropanol. Cylindrical sample chambers are fabricated from polydimethylsiloxane (PDMS) sealed to a glass slide. For magnetic manipulation, we deposit rods into PDMS sample wells and place cover glass on top of the sample chamber to minimize fluid motion due to evaporation. We observe Janus rod manipulations using an inverted transmission optical microscope with a 50× air objective (Nikon). Video data are collected at 60 or 120 frames per second using a Pulnix PTM-6710CL camera and in-house video capture software (a schematic of the microscope setup is included in the supporting information, figure SI1 (stacks.iop.org/JPhysD/44/125001/mmedia)).

Magnetic Janus nanorods are actuated via a NdFeB rectangular magnet (K&J Magnetics, Jamison, Pennsylvania).

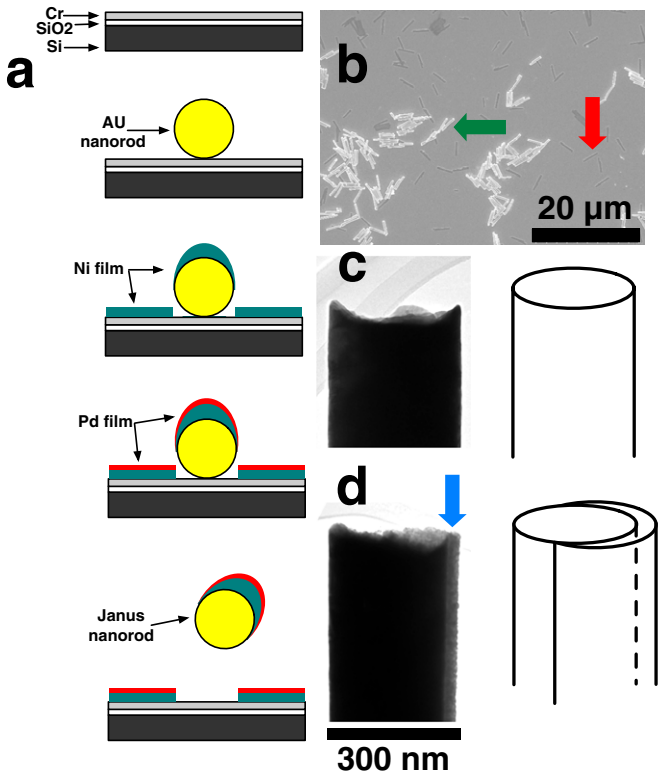

Figure 1. (*a*) Schematic of rod processing, showing a Cr-coated Si wafer, Au nanorod deposition onto the surface, Ni–Pd film deposition and Janus nanorod removal via sonication. (*b*) Partially removed Janus nanorods, showing a subset still adhered to the substrate surface (green arrow), while some rods have been lifted off during the sonication process (red arrow). TEM images of Au rod prior to (*c*) and after (*d*) thermally evaporated Janus layer (blue arrow). Cartoon representations are shown to the right.

This magnet is attached to a Barber-Colman inline gear motor driven by a constant external voltage source and positioned above the sample plane (see supporting information). The magnet is positioned such that the field strength at the sample plane is ∼30 G and the field direction is nearly parallel to the sample floor. The magnet is then rotated such that the field at the sample rotates in a plane nearly parallel to the floor, but tilted by some small angle θ. Motor drive voltage is varied to control the angular velocity of the magnetic Janus rods. Video tracking is performed via in-house software [43] to determine both angular and translational velocity. The magnet and rotating Janus rods have identical angular velocities, as evidenced by analysis of video data.

3. Results and discussion

3.1. Magnetic Janus nanorods

Direct transmission electron microscopy confirms the presence of the deposited layer on individual rods compared with untreated Au nanorod material (figures 1(*c*) and (*d*)). Approximately 60% of each nanorod's surface area (excluding rod faces) is covered by the deposited Ni–Pd layer. These rods exhibit ferromagnetic behaviour.

3.2. Rotation induces translation near a floor

While magnetic field gradients can be used to apply forces via passive translation (motion is exclusively in-plane translation), rotational manipulation is an active mode of translation during which rotation around some object axis produces in-plane translation. By rotating a magnetic field above Janus nanorods in solution and observing nanorods near the floor we observe two distinct modes of transport. A less stable, less frequently observed mode of locomotion relies on repeated, end-over-end rod tip friction interactions with the glass surface. During these interactions, direct contact between the rod tip and the glass substrate results in frictional forces which fix the tip at a specific substrate location. The field-aligning behaviour of the rod drives the bulk of the rod to pivot around the tip–substrate pivot point. For our magnetic Janus nanorods this 'walking' behaviour (figures 2(*d*)–(*f*)) is frequently short-lived (∼2–4 rod pivots, which we define as 'steps') and is terminated by irreversible adhesion to the glass surface. Single steps of this walking motion occur at discrete increments of nanorod length. Consequently, this mode of translation offers only low spatial resolution for nanorod positioning, with location being controllable by integer values of rod length. Detailed discussions of walking motion can be found elsewhere [44–46].

More commonly we observe 'crawling' motion (figures 2(*a*)–(*c*)) which is not dominated by tip–surface interactions, but propels the nanorod in incremental steps much smaller than the rod length. Like the walking mechanism, crawling also relies on near-surface friction in that the increased drag in the no-slip boundary near the substrate surface is directly responsible for the rod propulsion as it rotates. A small tilt out-of-plane results in symmetry-breaking, as the end of the rod which sweeps closer to the floor experiences an enhanced drag coefficient relative to the other half of the rod; the result is a net translation in a plane parallel to the floor. For clarification, it should be noted that there are three relevant planes for the motion we describe: (p1) the plane of the floor surface, (p2) the plane of nanorod translation (above and parallel to plane p1) and (p3) the plane in which the rod rotates (tilted by θ from planes p1 and p2, with $0^\circ < \theta < 20^\circ$). We later model this propulsion effect in detail. Because nanorod crawling relies on fluid-mediated frictional forces between the rod and the surface (as opposed to direct contact), the translational motion is incremental and has an individual crawl length (the distance travelled in one rod rotation) only a fraction of the rod length. These nanorod crawlers remain suspended above the sample floor due to electrostatic repulsive interactions between the ionic double layer around the rods and the negatively charged substrate; they can be actuated for tens of minutes without undergoing irreversible rod–substrate interactions. A video of each type of motion is available online as supporting information (video 1 (stacks.iop.org/JPhysD/44/125001/mmedia)). We show that nanorod translational velocity is linearly proportional to angular velocity and that rods can be manipulated independently along the x- and y-axes of a sample substrate by simple changes in the configuration of the applied magnetic field.

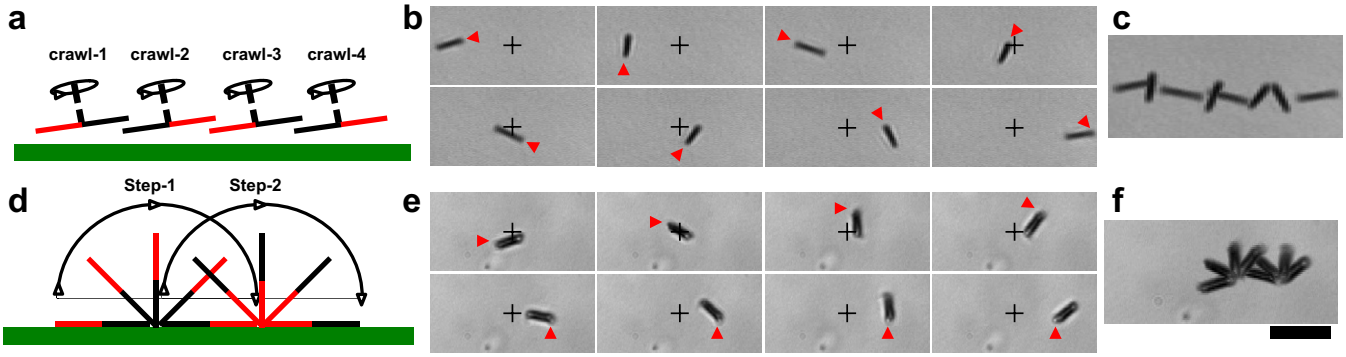

Figure 2. Two types of rod motion are observed. Crawling (*a*)–(*c*) and walking (*d*)–(*f*). Side view oriented cartoon representations (*a*), (*d*) indicate no-contact crawling versus end-over-end contact walking (note: black and red colour scheme in (*a*), (*d*) indicates the two effective magnetic poles on the nanorod). Microscope images taken from videos of crawling (*b*) and walking (*e*). The red triangle tracks the motion of a specific rod tip in the image sequence. Crosshairs have been added as points of reference. Minimum intensity projections (*c*), (*f*) show crawling and walking, respectively (supporting information video 1). Scale bar is 10 μm and refers to (*b*), (*c*), (*e*) and (*f*).

High resolution, variable speed, multidirectional control is compulsory for low Reynolds number swimming devices to be useful in microfluidic, biomedical and nano-scale assembly applications. We find that the translational velocity due to crawling varies directly with the angular velocity of the nanorod (figure 3). This translational motion is in the direction of $\omega \times \hat{z}$ where z represents the vertical axis. This translational motion is unidirectional (for a given rotation direction of the drive magnet) and oriented orthogonal to the angle θ (plane p3) of the nanorod tilt relative to the substrate. Reversal of the magnetic field rotational direction consequently reverses the rotational direction of the Janus nanorods (clockwise or counterclockwise), allowing control over translational direction ($+x$ or $-x$). Supporting information (video 2 (stacks.iop.org/JPhysD/44/125001/mmedia)) shows translational velocity varying with angular velocity, as well as directed translation in $+x$ and $-x$. Additionally, by changing the orientation (and therefore the orthogonal direction) of the magnet we are able to induce translation in any arbitrary direction. In order to demonstrate this control of motion, we manipulate a single nanorod along the path of the letters 'u–n–c' (figure 4, supporting information video 4 (stacks.iop.org/JPhysD/44/125001/mmedia)). Importantly, manipulation by this crawling mechanism makes it possible to control rod position and velocity in the lateral plane with a resolution of only a fraction of the rod length, as opposed to the walking mechanism, for which the translation resolution is limited to increments of rod length [44, 45].

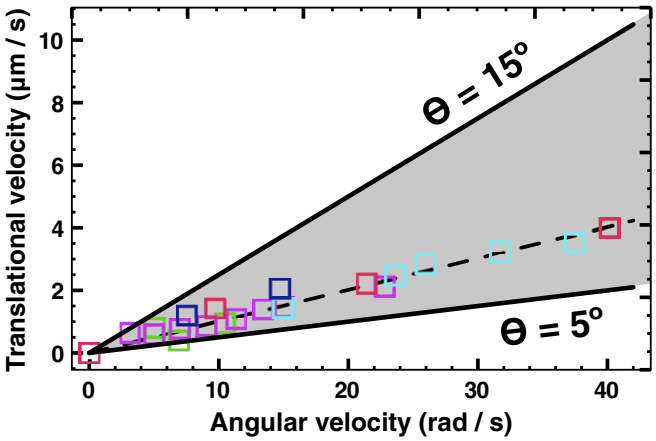

Figure 3. Measured translational (crawling) velocities of 5 magnetic Janus nanorods as a function of their angular velocities (data points), demonstrating a linear relationship. The dashed line is a linear fit to the data, with $v_t = 0.11\omega$. The solid lines represent the average translational velocity as a function of angular velocity, as predicted by our model, for rods with $\theta = 15^\circ$ and 5°. These relationships are calculated for rods sitting $h_0 = 0.9\,\mu$m above the glass floor, as determined by the average of 9 rod heights.

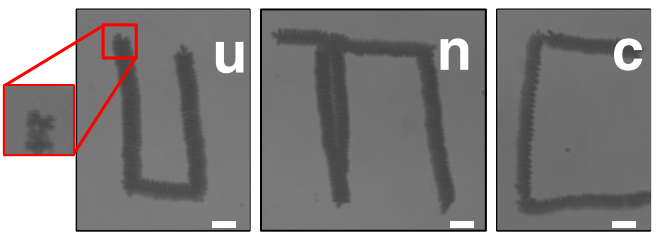

Figure 4. Minimum intensity projection of a single nanorod (crawling) manipulation, spelling out the letters 'u', 'n' and 'c'. Scale bars represent 10 μm. The full nanorod steering process is shown in supporting information video 4.

3.3. Microbead capture and manipulation

One intriguing potential application of nanorod translation is the ability to manipulate payloads in solution. To that end, we use Janus rods labelled on one side (the exposed Au surface) with 1,6-hexanedithiol to capture and translate a 1 μm metal-coated PS bead (see appendix). We load a sample chamber with both Janus nanorods and PS beads and controllably steer a chosen rod towards a PS bead suspended in solution near the surface (figure 5). Coarse rod manipulations are performed at translational velocities of ~2–4 μm s^{-1} (~20–40 rad s^{-1}). Once near the PS bead the rod angular velocity is slowed (~5–10 rad s^{-1}) to allow for fine positioning of the rod. When contact is made between the thiol coated face of the rod and the bead (figure 5(*c*)), a covalent bond is formed between the AuPd surface layer of the PS bead and the exposed thiol groups on the Au segment of the Janus rod.

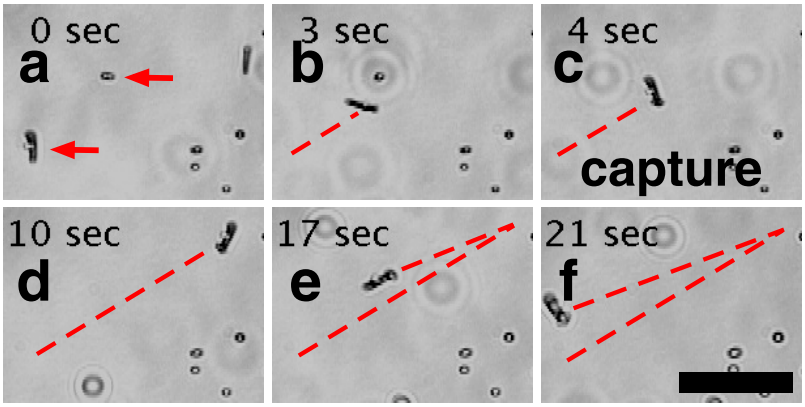

Figure 5. Dithiol-labelled Au–Ni Janus rod (lower arrow, (*a*)) approaches a pair of AuPd-coated PS beads (upper arrow, (*a*))(*a*)–(*b*), captures the beads via covalent linkage attached to the Au side of the rod (*c*), and is then manipulated towards the upper right corner of the frame (*d*), then towards the lower left corner of the frame (*e*)–(*f*). The broken red line indicates the path of the Janus nanorod. Scale bar represents 20 μm. The full process is shown in supporting information video 5.

Manipulation of chemically unmodified Janus rods into contact with AuPd-coated PS beads results in no observable binding interaction. After capture of a PS bead we observe no change in nanorod response to the rotating magnetic field, indicating that the presence of a bead payload does not perturb the translation mechanism measurably (supporting information video 5 (stacks.iop.org/JPhysD/44/125001/mmedia) shows bead approach, capture, and subsequent manipulation). As we discuss next, the cargo dimensions do play a role in the mechanism at work for cargo manipulation. However, the impact of cargo size on nanorod rotation is beyond the scope of the present research.

3.4. Single-cell manipulation

As a final, biologically relevant example of controllable manipulation, we also demonstrate directed single-cell translation using our magnetic Janus nanorods. Although this cell guidance mechanism does not rely specifically on Janus nanorod crawling, like nanorod crawling it allows for multidirectional translation of individual cells with spatial resolution (hundreds of nanometres) significantly smaller than the dimensions of the cell being manipulated (10–15 μm).

In general, a sphere rotating near but not in direct contact with a surface will translate in a plane parallel to that surface [47–49]. We use HBE-16 cells (see appendix) with diameters between 10 and 15 μm and couple our nanorods to them via nonspecific binding to membrane proteins. After cell-nanorod mixing in phosphate buffered saline (PBS) the solution is deposited into PDMS wells for magnetic manipulation. All manipulations are performed in PBS. During experimentation, cell-nanorod constructs settle near the surface with a variety of orientations. Optical microscopy indicates that HBE-16 cells in solution are indeed approximately spherical. We suggest that this sphere-spinning mechanism, as motivated by the field-aligning behaviour of the Janus nanorods, leads to controllable single-cell translational manipulation near the surface of the glass slide substrate. Indeed, in all cases rotation of the actuating permanent magnet results in cell rotation and subsequent translation. It is important to note that the resulting directed cell translation, like nanorod crawling, exhibits high resolution (less than the nanorod length) and controllability (figure 6). As the efficacy of this method relies heavily on the magnetization M of the nanorod, rods with larger amounts of magnetic material are preferred for the manipulation of cell-sized payloads. For example, pure Ni rods would prove more effective at single-cell manipulation as the field-aligning behaviour of our Janus rods utilizes only a 50 nm thick hemispherical layer of magnetic material.

One advantage of Janus rods is their highly tunable and user-specific composition. While Ni is not well tolerated by cells, our technique for the fabrication of high-aspect-ratio magnetic Janus rods makes it possible to conceal the ferromagnetic Ni layer by integrating materials with decreased cytotoxicity. Ultimately, materials more suitable for long-term biocompatibility, such as hydroxyapatite [50], may serve as candidates for Janus rod fabrication. We have demonstrated manoeuverability of magnetically actuable magnetic nanorod swimmers and demonstrated their ability to manipulate payloads with sizes of 1 μm and $\sim$10 μm. We now turn to modelling the operating propulsion mechanism for these nanorod crawlers.

3.5. Hydrodynamic model for nanorod crawling

In this study, symmetry is broken by a combination of nanorod tilt induced by an off-axis magnetic field and the boundary effect of the lower glass surface (floor). We see nanorods undergoing crawling translation near the floor of the sample chamber, where the no-slip boundary condition of the floor results in an enhanced drag coefficient. Since the drag coefficient is larger near the floor, the tilted rotation of the rod results in frictional asymmetry and thus a net translation. Here, we use resistive force theory [51] to explain this motion.

A ferromagnetic rod driven by a rotating magnetic field in a viscous fluid will rotate at the same angular velocity as the magnetic field as long as the angular velocity of the applied field, ω (rad s^{-1}), is less than the critical velocity of the rod-fluid system, $\omega_c = \xi/\gamma$, where ξ is the magnetic torque on the rod and γ is the drag coefficient of the rod [52]. For our

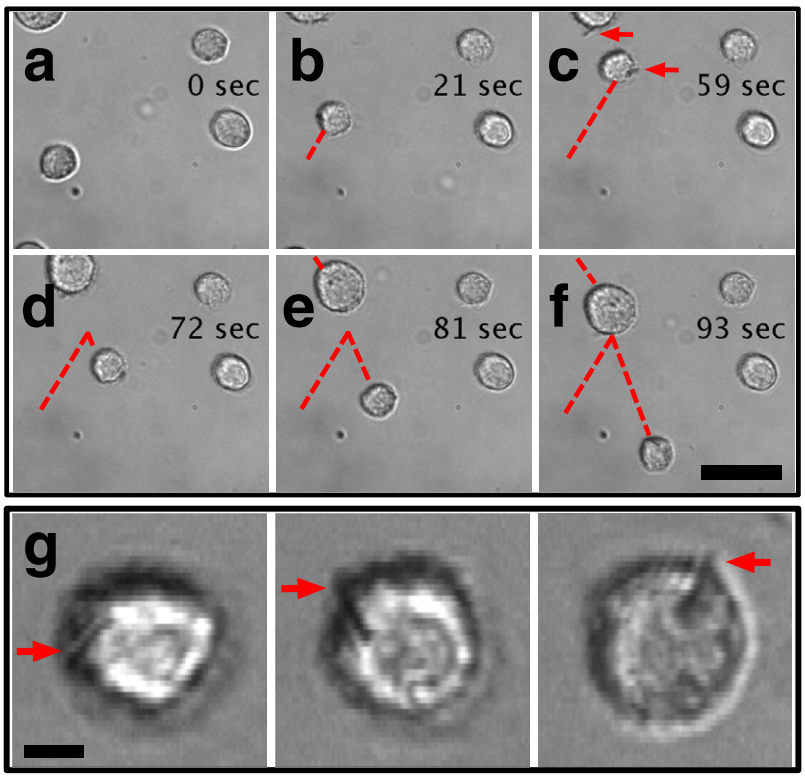

Figure 6. A human bronchial epithelial cell being manipulated by a single nanorod. In (*a*)–(*c*), magnet rotation is clockwise and the cell moves towards the top right of the field of view. In (*d*)–(*f*), the magnet position is changed and direction is reversed and, consequently the cell is manipulated towards the lower right of the field of view. Three frames (*g*) show the changing orientation of the Janus rod (arrows) relative to the cell under the rotating magnetic field. Scale bars represent 30 μm (*a*)–(*f*) and 5 μm (*g*). The full process is shown in supporting information video 6 (stacks.iop.org/JPhysD/44/125001/mmedia).

system, $\omega_c \approx 10^4\,\mathrm{rad\,s^{-1}}$, which is much greater than typical values of ω in this work (typically 2–50 $\mathrm{rad\,s^{-1}}$), and so we can assume that $\omega_{\mathrm{magnet}} = \omega_{\mathrm{rod}} \equiv \omega$.

The net velocity of a segment of the rod a distance ρ from its centre can be described as the vector sum of its translational and rotational velocities (inset, figure 7(*a*)). Decomposing this velocity v into components both parallel and perpendicular to the long axis of the rotating rod, we find

$$v_\perp = \omega\rho + v_t\cos(\omega t), \qquad v_\parallel = v_t\sin(\omega t) \tag{1}$$

where ω is the rod angular velocity, v_t is the rod translational velocity and t is time. We also assume that the angle between the plane of rotation and the horizontal, θ, is small, as determined by observation of apparent rod length during a rotation. The differential drag force on a segment of the rod a distance ρ from the center is then given by

$$\mathrm{d}F_\perp = \gamma_\perp v_\perp \mathrm{d}\rho, \qquad \mathrm{d}F_\parallel = \gamma_\parallel v_\parallel\,\mathrm{d}\rho \tag{2}$$

where $\gamma_\perp$ and $\gamma_\parallel$ are the drag coefficients in the perpendicular and parallel directions, respectively. Due to symmetry considerations, there is no net translation in the y- and z-directions. In the x-direction, the net force is given by the sum of the x-components of $\mathrm{d}F_\perp$ and $\mathrm{d}F_\parallel$ as the rod rotates at constant angular velocity

$$\mathrm{d}F_x = \mathrm{d}F_\perp\cos(\omega t) + \mathrm{d}F_\parallel\sin(\omega t). \tag{3}$$

In this model we make use of the drag coefficients given by Hunt *et al* [53]

$$\mathrm{d}F_x = \frac{2\pi\eta}{\cosh^{-1}\left(\frac{h(\rho,t)}{r}\right)}[2\omega\rho\cos(\omega t) + v_t(1+\cos^2(\omega t))]\,\mathrm{d}\rho \tag{4}$$

where η is the viscosity of the fluid, r is the radius of the rod and h is the height of each element of the rod above the floor, which is a function of both ρ and t. The height of the rod as it rotates can be expressed by $h(\rho, t) = h_0 + \rho\sin\theta\cos(\omega t)$, where h_0 is the height of the centre of the rod and θ is the angle by which the plane of rotation is tilted from the horizontal. Since the rod rotates in a low-Re fluid, inertial forces are negligible and the net force on the swimmer in the x-direction is zero at all times. Thus,

$$F_x = 0 = \int \frac{2\pi\eta[2\omega\rho\cos(\omega t) + v_t(1+\cos^2(\omega t))]}{\cosh^{-1}[(1/r)(h_0 + \rho\sin\theta\cos(\omega t))]}\mathrm{d}\rho. \tag{5}$$

Integration yields an expression for the translational velocity of the rod as a function of time, $v_t(t)$:

$$v(t) = \frac{2\omega csc\theta}{3+\cos(2\omega t)}[2h\mathrm{Shi}(\cosh^{-1}A) - r\mathrm{Shi}(2\cosh^{-1}A) - 2h\mathrm{Shi}(\cosh^{-1}B) + r\mathrm{Shi}(2\cosh^{-1}B)][\mathrm{Shi}(\cosh^{-1}A) - \mathrm{Shi}(\cosh^{-1}B)]^{-1} \tag{6}$$

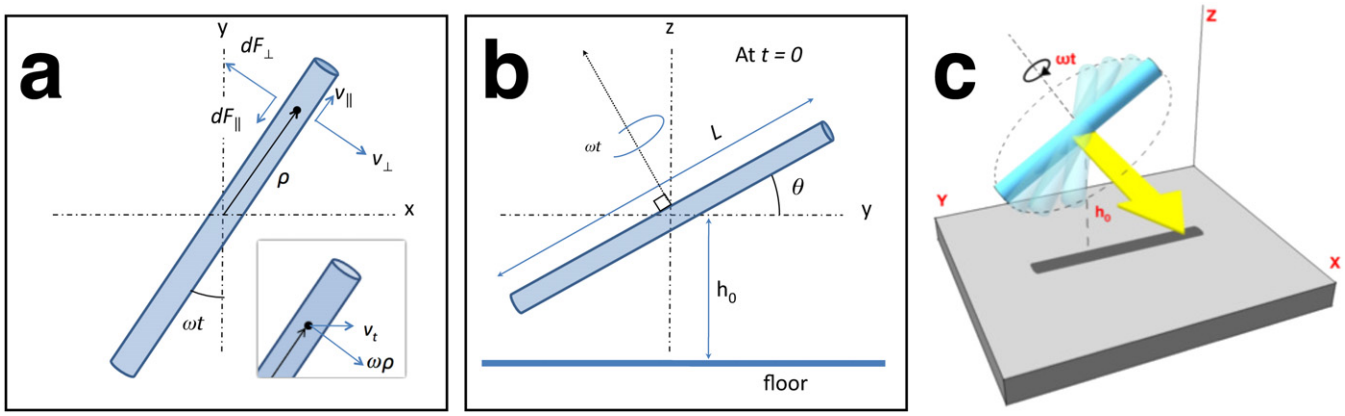

Figure 7. Top (*a*) and side (*b*) views of the rotating nanorod. The rod rotates clockwise with constant angular velocity, ω, and moves in the x-direction with a translational velocity $v(t)$ (*a*, inset). A point on the rod an arbitrary distance ρ from the centre has components of velocity both parallel and perpendicular to the axis of the rod, which generate differential drag forces in the opposite direction. The plane of rotation is tilted away from the horizontal by an angle θ, resulting in an enhanced drag coefficient for the segments of the rod nearest to the lower surface. The height of the centre of the rod above the floor is denoted by h_0. The perspective image (*c*) shows the rod as it travels through a fraction of its rotation in the vicinity of the floor. An animated artist's rendering of (*c*) is available in supporting information video 3 (stacks.iop.org/JPhysD/44/125001/mmedia).

where Shi(x) is the hyperbolic sine integral and

$$A = \frac{2h - L\cos(\omega t)\sin\theta}{2r}, \quad B = \frac{2h + L\cos(\omega t)\sin\theta}{2r}. \quad (7)$$

The average translational velocity can be determined by numerical integration over a quarter-period; however, since $v_t(t)$ is very nearly sinusoidal, $v_{avg} \sim v_{max}/2 = v_t(0)/2$ yields a good approximation. The average translational velocity is independent of viscosity, as expected for a low-Re swimmer, and increases linearly with angular velocity, as observed in our experiments.

Using experimentally determined values or value ranges for L, r, θ and h_0 we evaluate the translational velocity versus angular velocity data with respect to our model. L and r are experimentally determined to be 5.5±0.1 μm and 150±30 nm, respectively (SEM imaging). An average rod height of $h_0 = 1.0 \pm 0.2\,\mu$m is determined using a piezo stage (Mad City Labs, Madison, Wisconsin) to focus on rods in motion, then compare these heights with nearby rods adhered to the sample floor. We determine a range for θ by analysis of rod apparent length during each frame of a rod rotation, which yields an upper bound of $\theta_{max} = 20°$.

Using the specified L, r and h_0 values we evaluate v_t versus ω for $\theta = 5°$ and 15°. For $\theta = 5°$ and 15°, $v_t = 0.05\omega$ and 0.26ω, respectively (solid lines shown in figure 3). Our rods move with $v_t = 0.11\omega$, which is in agreement with the theoretical results shown in figure 3. This crawling mechanism allows for continuous control over nanorod position, as fractions of a rotation can be used to achieve high resolution, incremental advances in position. If the notion of individual steps are applied to these Janus nanorod crawlers then a rotation of π radians would serve as a useful representation of a single step. Using this measure of a step we can attribute a step size of 350 nm/step to the crawling mechanism, as implemented by our Janus crawlers. Changing the rod length, radius, and, most significantly, angle with respect to the floor, allows for the step length to be tuned to meet a specific set of micromanipulation requirements.

4. Conclusion

We present the fabrication of ferromagnetic Janus nanorods and utilize these materials to perform complex manoeuvers, covalent payload capture, and subsequent payload manipulation. Additionally, we demonstrate that these nanorods, when attached to cells, are capable of rotating the cell and thereby producing directed single-cell translation. We model the propulsion mechanism using resistive force theory and show that a small tilt out of the plane of the floor is all that is required to produce hydrodynamic swimming. Future applications of these rods may make use of their combined Janus structuring and magnetic properties for applications such as in-solution magnetic separation.

Acknowledgments

The authors thank Dr Amar Kumbhar of the Chapel Hill Nanofabrication Laboratories for technical TEM assistance, as well as Dr Jeremy Cribb for his work in developing the image capture software used for these experiments.

Appendix A. Experimental procedures

We prepare Janus rods for bead capture by gentle vortexing of rods in 1,6-hexanedithiol (1 mM in ethanol), followed by centrifugation and subsequent rinsing (10×) in ethanol. PS beads (1 μm diameter, Molecular Probes) are prepared by first diluting stock solutions 1/1000 in ethanol (~4.2 × 10^{-3}% solids). These dilutions are sonicated for 30 min, deposited onto plasma-cleaned glass slides and sputter-coated with ~10 nm 80Au–20Pd films. Beads are collected via substrate sonication in ethanol (20 s, 12 W), after which they are centrifuged and rinsed.

Human transformed bronchial epithelial cells (HBE-16) are grown in T-25 cell culture flasks. The cells are washed with PBS twice per week and maintained with Dulbecco's

Modified Eagle Medium/F12 (DMEM/F12) with 5% fetal bovine serum. HBE-16 cells are routinely passaged upon reaching confluence. In preparation for Janus nanorod manipulation, these cells are trypsinized, spun into a pellet and resuspended in DMEM/F12 at a concentration of about 2 million cells/ml. Cells are incubated with Janus nanorods under gentle vortex mixing for 1 h prior to magnetic manipulation. The manipulation experiments presented here make use of nonspecific cell-nanorod binding [54], which mechanically couples the cell membrane to the rods. Although not all cell-nanorod interactions result in irreversible cell binding and particle adhesion, successfully bound nanorods remain intact for the duration of these cell manipulation experiments.

References

[1] Ebbens S J and Howse J R 2010 In pursuit of propulsion at the nanoscale *Soft Matter* **6** 726–738

[2] Ozin G A, Manners I, Fournier-Bidoz S and Arsenault A 2005 Dream nanomachines *Adv. Mater.* **17** 3011–8

[3] Sundararajan S, Lammert P E, Zudans A W, Crespi V H and Sen A 2008 Catalytic motors for transport of colloidal cargo *Nano Lett.* **8** 1271–6

[4] Sundararajan S, Sengupta S, Ibele M E and Sen A 2010 Drop-off of colloidal cargo transported by catalytic pt–au nanomotors via electrochemical stimuli *Small* **6** 1479–82

[5] Burdick J, Laocharoensuk R, Wheat P M, Posner J D and Wang J 2008 Synthetic nanomotors in microchannel networks: directional microchip motion and controlled manipulation of cargo *J. Am. Chem. Soc.* **130** 8164–5

[6] Kline T R, Paxton W F, Mallouk T E and Sen A 2005 Catalytic nanomotors: remote-controlled autonomous movement of striped metallic nanorods *Angew. Chem. Int. Edn* **44** 744–6

[7] Mallouk T E, Sen A and Paxton W F 2005 Catalytic movement of nanoscale objects *Chem. Eur. J.* **11** 6462–70

[8] Mirkovic T, Zacharia N S, Scholes G D and Ozin G A 2010 Fuel for thought: chemically powered nanomotors out-swim nature's flagellated bacteria *ACS Nano* **4** 1782–9

[9] Paxton W F, Sundararajan S, Mallouk T E and Sen A 2006 Chemical locomotion *Angew. Chem. Int. Edn* **45** 5420–9

[10] Paxton W F, Kistler K C, Olmeda C C, Sen A, St Angelo S K, Cao Y, Mallouk T E, Lammert P E and Crespi V H 2004 Catalytic nanomotors: autonomous movement of striped nanorods *J. Am. Chem. Soc.* **126** 13424–31

[11] Valadares L F, Tao Y-G, Zacharia N S, Kitaev V, Galembeck F, Kapral R and Ozin G A 2010 Catalytic nanomotors: self-propelled sphere dimers *Small* **6** 565–72

[12] Zacharia N S, Sadeq Z S and Ozin G A 2009 Enhanced speed of bimetallic nanorod motors by surface roughening *Chem. Commun.* **2009** 5856–8

[13] Zhang L, Abbott J J, Dong L, Peyer K E, Kratochvil B E, Zhang H, Bergeles C and Nelson B J 2009 Characterizing the swimming properties of artificial bacterial flagella *Nano Lett.* **9** 3663–7

[14] Zhang L, Abbott J J, Dong L, Kratochvil B E, Bell D and Nelson B J 2009 Artificial bacterial flagella: fabraction and magnetic control *Appl. Phys. Lett.* **94** 064107

[15] Zhang L, Petit T, Lu Y, Kratochvil B E, Peyer K E, Pei R, Lou J and Nelson B J 2010 Controlled propulsion and cargo transport of rotating nickel nanowires near a patterned solid surface *ACS Nano* **4** 6228–34

[16] Sing C E, Schmid L, Schneider M F, Franke T and Alexander-Katz A 2010 Controlled surface-induced flows from the motion of self-assembled colloidal walkers *Proc. Natl Acad. Sci. USA* **107** 535–40

[17] Ghosh A and Fischer P 2009 Controlled propulsion of artificial magnetic nanostructured propellers *Nano Lett.* **9** 1922–33

[18] Tierno P, Golestanian R, Pagonabarraga I and Sagués F 2008 Controlled swimming in confined fluids of magnetically actuated colloidal rotors *Phys. Rev. Lett.* **101** 218304

[19] Garstecki P, Tierno P, Weibel D B, Sagues F and Whitesides G M 2009 Propulsion of flexible polymer structures in a rotating magnetic field *J. Phys.: Condens. Matter* **21** 204110

[20] Tierno P, Güell O, Sagués F, Golestanian R and Pagonabarraga I 2010 Controlled propulsion in viscous fluids of magnetically actuated colloidal doublets *Phys. Rev.* E **81** 011402

[21] Baudry J, Fermigier M, Bibette J, Dreyfus R, Stone H A and Roper M L 2005 Microscopic artificial swimmers *Nature* **437** 862

[22] Tierno P, Golestanian R, Pagonabarraga I and Sagués F 2008 Magnetically actuated colloidal microswimmers *J. Phys. Chem.* B **112** 16525–8

[23] Purcell E M 1977 Life at low Reynolds number *Am. J. Phys.* **45** 3–11

[24] Childress S 1981 *Mechanics of Swimming and Flying* (Cambridge: Cambridge University Press) ISBN 0521280710

[25] Najafi A and Golestanian R 2004 Simple swimmer at low Reynolds number: Three linked spheres *Phys. Rev.* E **69** 062901

[26] Becker L E, Koehler S A and Stone H A 2003 On self-propulsion of micro-machines at low Reynolds number: Purcells three-link swimmer *J. Fluid Mech.* **490** 15–35

[27] Keaveny E E and Maxey M R 2008 Spiral swimming of an artificial micro-swimmer *J. Fluid Mech.* **598** 293–319

[28] Belovs M and Cebers A 2009 Ferromagnetic microswimmer *Phys. Rev.* E **79** 051503

[29] Najafi A and Golestanian R 2005 Propulsion at low Reynolds number *J. Phys.: Condens. Matter* **17** S1203–8

[30] Casagrande C and Veyssie M 1988 Janus beads—realization and 1st observation of interfacial properties *C. R. Acad. Sci.* **306** 1423–5

[31] Attenborough K, Hart R, Lane S J, Alper M and Schwarzacher W 1995 Magnetoresistance in electrodeposited Ni–Fe–Cu/Cu multilayers *J. Magn. Magn. Mater.* **148** 335–6

[32] Elnathan R, Kantaev R and Patolsky F 2008 Synthesis of hybrid multicomponent disklike nanoparticles *Nano Lett.* **8** 3964–72

[33] Wang L, Yu-Zhang K, Metrot A, Bonhomme P and Troyon M 1996 Tem study of electrdeposited ni/cu multilayers in the form of nanowires *Thin Solid Films* **288** 86–9

[34] Wildt B, Mali P and Searson P C 2006 Electrochemical template synthesis of multisegment nanowires: Fabrication and protein functionalization *Langmuir* **22** 10528–34

[35] Hurst S J, Payne E K, Qin L and Mirkin C A 2006 Multisegmented one-dimensional nanorods prepared by hard-template synthetic methods *Angew. Chem. Int. Edn* **45** 2672–92

[36] Qin L D, Park S, Huang L and Mirkin C A 2005 On-wire lithography *Science* **309** 113–5

[37] Martin C R and Baker L A 2005 Expanding the molecular electronics toolbox *Science* **309** 67–8

[38] Qin L D, Banholzer M J, Xu X Y, Huang L and Mirkin C A 2007 Rational design and synthesis of catalytically driven nanorotors *J. Am. Chem. Soc.* **129** (48) 14870–1

[39] Wang Y, Fei S-T, Byun Y-M, Lammert P E, Crespi V H, Sen A and Mallouk T E 2009 Dynamic interactions between fast microscale rotors *J. Am. Chem. Soc.* **131** 9926–7

[40] Qin L, Banholzer M J, Millstone J E and Mirkin C A 2007 Nanodisk codes *Nano Lett.* **7** 3849–53

[41] Hangarter C M, Rheem Y, Yoo B, Yang E H and Myung N V 2007 Hierarchical magnetic assembly of nanowires *Nanotechnology* **18** 205305
[42] Hangarter C M and Myung N V 2005 Magnetic alignment of nanowires *Chem. Mater.* **17** 1320–4
[43] Taylor R M 2009 Video spot tracker http://cismm.cs.unc.edu/downloads/?dl_cat=3
[44] Zhao Y and Zeng H 2009 Rotational maneuver of ferromagnetic nanowires for cell manipulation *IEEE Trans. Nanobiosci.* **8** 226–36
[45] Zeng H, Ebel J and Zhao Y 2009 Rapid cell manipulation by rotating nanowires *Mater. Res. Soc. Symp. Proc.* **1139** 25–30
[46] Morimoto H, Ukai T, Nagaoka Y, Grobert N and Maekawa T 2008 Tumbling motion of magnetic particles on a magnetic substrate induced by a rotational magnetic field *Phys. Rev.* E **78** 021403 8
[47] Blake J R 1971 A note on the image system for a stokeslet in a no-slip boundary *Proc. Camb. Phil. Soc.* **70** 303–10
[48] Goldman A J, Cox R G and Brenner H 1967 Slow viscous motion of a sphere parallel to a plane wall: I. Motion through a quiescent fluid *Chem. Eng. Sci.* **22** 637–51
[49] Reichert M and Stark H 2004 Hydrodynamic coupling of two rotating spheres trapped in harmonic potentials *Phys. Rev.* E **69** 031407
[50] Balasundaram G, Sato M and Webster T J 2006 Using hydroxyapatite nanoparticles and decreased crystallinity to promote osteoblast adhesion similar to functionalizing with rgd *Biomaterials* **27** 2798–805
[51] Gray J and Hancock G J 1955 The propulsion of sea-urchin spermatozoa *J. Exp. Biol.* **32** 802–14
[52] Urena E B, Mei Y, Coric E, Makarov D, Albrecht M and Schmidt O G 2009 Fabrication of ferromagnetic rolled-up microtubes for magnetic sensors on fluids *J. Phys. D: Appl. Phys.* **42** 055001
[53] Hunt A J, Gittes F and Howard J 1994 The force exerted by a single kinesin molecule against a viscous load *Biophysical J.* **67** 766–81
[54] Hultgren A, Tanase M, Chen C S, Meyer G J and Reich D H 2003 Cell manipulation using magnetic nanowires *J. Appl. Phys.* **93** 7554–6